Available online at www.sciencedirect.com
ScienceDirect
Journal of Theoretical Biology 248 (2007) 64–80
Journal of Theoretical Biology
www.elsevier.com/locate/yjtbi

A mathematical model of fluid secretion from a parotid acinar cell

Elan Gin[a,*], Edmund J. Crampin[b], David A. Brown[c], Trevor J. Shuttleworth[c], David I. Yule[c], James Sneyd[a]

[a]*Department of Mathematics, The University of Auckland, Private Bag 92019, Auckland, New Zealand*
[b]*Auckland Bioengineering Institute and Department of Engineering Science, The University of Auckland, Private Bag 92019, Auckland, New Zealand*
[c]*Department of Pharmacology and Physiology and the Center for Oral Biology, University of Rochester Medical Center, Rochester, NY 14642, USA*

Received 4 October 2006; received in revised form 4 April 2007; accepted 26 April 2007
Available online 3 May 2007

Abstract

Salivary fluid secretion is crucial for preventing problems such as dryness of mouth, difficulty with mastication and swallowing, as well as oral pain and dental cavities. Fluid flow is driven primarily by the transepithelial movement of chloride and sodium ions into the parotid acinus lumen. The activation of Cl^- channels is calcium dependent, with the average elevated calcium concentration during calcium oscillations increasing the conductance of the channels, leading to an outflow of Cl^-. The accumulation of NaCl in the lumen drives water flow by osmosis. We construct a mathematical model of the calcium concentration oscillations and couple this to a model for Cl^- efflux. We also construct a model governing fluid flow in an isolated parotid acinar cell, which includes a description of the rate of change of intracellular ion concentrations, cell volume, membrane potential and water flow rate. We find that $[Ca^{2+}]$ oscillations lead to oscillations in fluid flow, and that the rate of fluid flow is regulated by the average calcium concentration and not the frequency of the oscillations.

Keywords: Mathematical model; Salivary fluid secretion; Parotid acinar cells; Intracellular calcium; Cl^- channels and fluxes

1. Introduction

An adequate supply of saliva is important to maintaining oral health. Reduced salivary flow can cause complaints such as dryness of the mouth, difficulty with mastication and swallowing. Oral pain, increased dental cavities and infections are also complaints associated with decreased salivation. Salivary gland dysfunction is also observed in diseases such as Sjögren's syndrome. For these reasons, it is important to understand the mechanisms underlying salivary secretion.

Three pairs of major salivary glands (parotid, submandibular and sublingual) are found in mammals. The glands consist of secretory end pieces, the acini, gathered in clusters at the end of a duct. The parotid acinar cells secrete the primary salivary fluid as well as most of the salivary proteins. The sublingual gland secretes water and electrolytes along with mucins, while the submandibular glands secrete both serous and mucous products. The ductal cells secrete some proteins and modify the ionic composition of the saliva. Humans secrete more than a litre of saliva each day, mostly from the parotid and submandibular glands.

Salivary fluid secretion is a two-stage process, first proposed by Thaysen et al. (1954). In this first stage, saliva is formed in the acinar lumen. This primary fluid, which is isotonic or slightly hypertonic to the interstitial concentration, is then modified in the salivary ducts by removing sodium and chloride and adding potassium and bicarbonate to produce a hypotonic fluid which enters the mouth.

Fig. 1 shows two schematic diagrams of a parotid acinar cell and the various mechanisms which establish an osmotic gradient to drive water flow. In both diagrams, the mechanisms for driving water flow are the same; they differ in the water flow pathway. For a review of the three different mechanisms proposed for driving water flow, see Cook and Young (1989b), Nauntofte (1992), Turner et al.

*Corresponding author. Tel.: +64 9 3737599x85745; fax: +64 9 3737457.
E-mail address: elan@math.auckland.ac.nz (E. Gin).

0022-5193/$ - see front matter © 2007 Elsevier Ltd. All rights reserved.
doi:10.1016/j.jtbi.2007.04.021

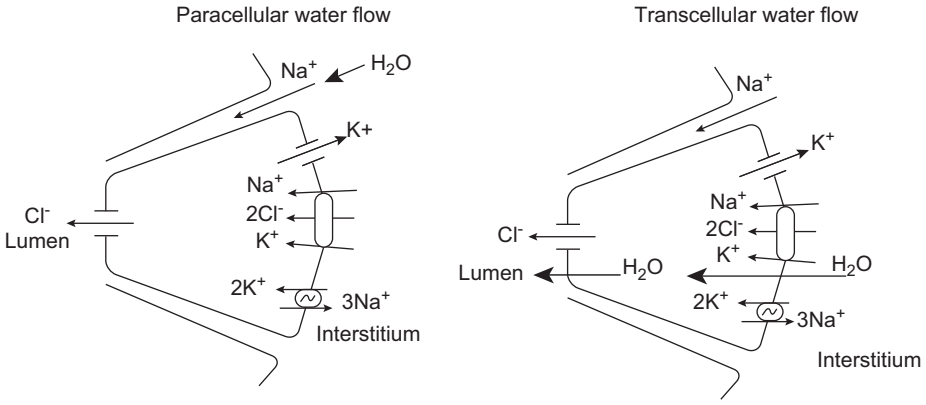

Fig. 1. Model for salivary fluid secretion. The accumulation of Cl^- in the lumen creates a driving force for water flow into the lumen. In the left panel, water flow is via a paracellular pathway. The right panel shows water flow via a transcellular pathway.

(1993) and Turner and Sugiya (2002). The model used in this paper includes four mechanisms for ion movement: a $Na^+-K^+-ATPase$, a $Na^+-K^+-2Cl^-$ cotransporter, a Ca^{2+}-activated K^+ channel located in the basolateral membrane and a Ca^{2+}-activated Cl^- channel located in the apical membrane. Fluid secretion is thought to arise from the concerted actions of these four ion-movement mechanisms. The activation of Cl^- channels by Ca^{2+} causes a transepithelial movement of Cl^- into the lumen. In order to maintain an electrical driving force, K^+ leaves the cell via the K^+ channel. The distinct spatial distribution of the two channels, with the Cl^- channel located in the apical membrane and the K^+ channel located in the basolateral membrane, means that K^+ leaves the cell into the interstitium. Therefore, as the lumen is negative, this pulls Na^+ ions into the lumen. It is the accumulation of NaCl in the lumen which is the main driving force for fluid secretion. Na^+ ions are thought to follow the Cl^- by diffusing from the interstitium to the lumen, across the tight junctions of the acinar cell. A K^+ flux into the lumen is also possible. A summary of the experimental evidence for this can be found in Cook and Young (1989a). We detail the potential influence of this flux in the discussion section. The osmotic gradient created by the NaCl in the lumen drives the flux of water into the lumen. There are two routes by which water is thought to move into the lumen. The panel on the left of Fig. 1 shows water flowing via a paracellular pathway through the tight junction complex into the lumen, while the panel on the right shows water flow into the lumen through the cell via the cytoplasm. The two pathways are described in further detail in Section 3.

Ca^{2+} signalling plays an important role in controlling many physiological processes, and here, Ca^{2+} is the main signalling pathway in the regulation of salivary fluid secretion. Sustained levels of fluid secretion are accomplished by a sustained elevation of $[Ca^{2+}]$. However, prolonged periods of elevated Ca^{2+} levels are toxic to cells, so instead, $[Ca^{2+}]$ oscillations are used to maintain an average elevated $[Ca^{2+}]$. This activates the K^+ and Cl^- channels, which in turn leads to an activation of the transporters. These concerted activities lead to water flow into the lumen and resulting salivary fluid secretion. We first model the processes shown in Fig. 1 in an isolated parotid acinar cell. Next we construct a model describing the Ca^{2+} dynamics in a parotid acinar cell. The two models are then coupled to investigate the water flow. We also investigate whether the frequency of the $[Ca^{2+}]$ oscillations affects the average water flow rate. The ultimate aim of this model is to predict what is likely to happen if some of the processes affecting salivary secretion are disabled. For example, Evans et al. (2000) studied salivary secretion in mice in which the gene for $Na^+-K^+-2Cl^-$ cotransporter had been disrupted, and found that the stimulated salivary flow rates were only 40% of the rate of normal littermates. This shows there is activity from alternative transporters, mainly Na^+/H^+ and Cl^-/HCO_3^- exchangers, and we wish to understand these interactions quantitatively. Although detailed investigations of this type are beyond the scope of this present paper, which focuses on model construction and validation, the work here is a necessary first step for such studies.

2. Mechanisms underlying fluid secretion

In this section, we construct a mathematical model incorporating the channels and cotransporters in Fig. 1. The possible routes for water flow are paracellular, transcellular or a combination of water flow between and through the cells. In this work we consider transcellular water flow although we have also performed simulations for paracellular flow with very similar results. Water flow is controlled by changes in the osmolarity of the cell and the lumen. We let the variables [Cl], [Na], [K], [Ca] denote the ion concentrations with subscripts i, e and l denoting the intracellular, interstitial and luminal compartments, respectively. The interstitial concentrations are fixed at $[Cl]_e = 115\,mM$, $[Na]_e = 150\,mM$ and $[K]_e = 5\,mM$. We also keep track of the changes in the luminal chloride concentration; this is denoted by $[Cl]_l$. The cell volume, w,

is also a variable. We discuss each of the ion transport mechanisms shown in Fig. 1 in the following sections.

2.1. Cl^- channel

The transepithelial movement of Cl^- is the main driving force for fluid secretion by the salivary acinar cells. The activation of the Cl^- channel is triggered by increased $[Ca^{2+}]$. The Cl^- channel model we use is based on one developed for rat parotid acinar cells by Arreola et al. (1996), which incorporates two sequential Ca^{2+} binding steps followed by a transition to an open state. The first two steps are assumed to be in equilibrium giving a steady-state open probability:

$$P_{Cl} = \frac{1}{1 + K_2(K_1^2/[\mathrm{Ca}]_i^2 + K_1/[\mathrm{Ca}]_i + 1)}.$$

The equilibrium constants K_1 and K_2 are voltage dependent and are given by

$$K_1 = 234\exp\left(\frac{-0.13FV_m}{RT}\right)\mathrm{nM}, \quad K_2 = 0.58\exp\left(\frac{-0.24FV_m}{RT}\right).$$

We have modified K_1 from the model used by Arreola et al. (1996), in which $K_1 = 214\exp(-0.13FV_m/RT)$, to obtain a small open probability at a resting $[Ca^{2+}]$ of 0.05 μM in our model. Because the water flow is governed by the Cl^- flux into the lumen, we require a small flux so that the resting water flow rate is low. The total current through the Cl^- channel is then given by

$$I_{Cl} = g_{cl}P_{Cl}(V_m - V_{Cl}),$$

where g_{Cl} is the maximum whole cell conductance for Cl^-,

$$V_{Cl} = \frac{RT}{z_{Cl}F}\log\left(\frac{[\mathrm{Cl}]_l}{[\mathrm{Cl}]_i}\right)$$

is the Nernst potential for Cl^-, $R = 8.315\,\mathrm{J\,mol^{-1}\,K^{-1}}$, $T = 310\,\mathrm{K}$, $F = 96\,490\,\mathrm{C\,mol^{-1}}$ and $z_{Cl} = -1$ is the valence for Cl^-. The membrane potential is given by V_m with units of mV. We do not distinguish between apical and basolateral membrane potentials; the reason for this is discussed in Section 3. The maximum whole-cell chloride conductance, g_{Cl}, is 31.4 nS which is the average maximum conductance found by Arreola et al. (1996). We note that the driving force is linear, but the net flux is nonlinear because of the open probability term, which is a function of both calcium concentration and membrane potential. Fig. 5C of Arreola et al. (1996) shows the instantaneous current–voltage relationship in rat parotid cells to be linear. Thus, we use a linear current–voltage relationship rather than the more usual Goldman–Hodgkin–Katz equation.

2.2. K^+ channel

The family of Ca^{2+}-activated K^+ channels contains three types, characterised by small, intermediate and large conductances. Both the maxi-K class (large conductance) and intermediate conductance Ca^{2+}-activated K^+ channels (IK1) have been observed in parotid acinar cells. Thompson and Begenisich (2006) found that activation of IK1 channels inhibited maxi-K activity. For this reason, we include only an intermediate conductance, Ca^{2+}-activated K^+ channel.

The model used is the Hill equation, where the open probability is given by

$$P_{K_0} = \frac{1}{1 + (K_d/[\mathrm{Ca}]_i)^{n_H}},$$

where K_d is the dissociation constant and n_H is the Hill coefficient. Takahata et al. (2003) investigated the IK1 channels in bovine parotid acinar cells and fitting the Hill equation to their data, they obtained $K_d = 0.43\,\mu\mathrm{M}$ and $n_H = 2.54$ at $-55\,\mathrm{mV}$. They found that K_d was voltage-independent. We used $K_d = 0.182\,\mu\mathrm{M}$ and $n_H = 2.0$, which were chosen to give a small current at resting $[Ca^{2+}]$. As there is very little Cl^- flux at steady-state, there must also be very little K^+ flux, as the movement of K^+ out of the cell is to balance the outgoing Cl^-. The total current through the K^+ channels is given by

$$I_K = g_K P_{K_0}(V_m - V_K),$$

where g_K is the maximum whole cell conductance for K^+ and

$$V_K = \frac{RT}{z_K F}\log\left(\frac{[\mathrm{K}]_e}{[\mathrm{K}]_i}\right)$$

is the Nernst potential for K^+ with $z_K = +1$. The parameter g_K was set at 11.58 nS which is slightly lower than the maximum whole-cell conductance of around 14 nS found by Thompson and Begenisich (2006).

2.3. $Na^+-K^+-ATPase$

The Na^+-K^+-ATPase maintains low $[Na^+]$ and high $[K^+]$ in the cell, relative to the interstitium. It does this by exchanging 3 Na^+ for 2 K^+, at the expenditure of ATP. The model used here is based on a 15-state model derived by Läuger and Apell (1986). A lumping-scheme was applied by Smith and Crampin (2004) to reduce the 15-state model to a 4-state representation of the Na^+-K^+ pump. We use this 4-state model and the resulting steady-state flux representation as in Smith and Crampin (2004):

$$v_{NaK} = \frac{\alpha_1^+\alpha_2^+\alpha_3^+\alpha_4^+ - \alpha_1^-\alpha_2^-\alpha_3^-\alpha_4^-}{\Sigma},$$

where the α_i^+ are the forward reaction steps and the α_i^- are the backward reaction steps for $i = 1, 2, 3, 4$; these are given in Appendix A. Details of Σ, thermodynamic considerations and voltage dependence partitioning can also be found in Appendix A. Parameter values are given in Table 1 and are taken from Smith and Crampin (2004).

Table 1
Parameter values for the $Na^+-K^+-ATPase$ taken from Smith and Crampin (2004) except [MgATP], [MgADP] and [Pi]

Rate constants			
k_1^+	$1050\,s^{-1}$	k_1^-	$172.1\,s^{-1}\,mM^{-1}$
k_2^+	$481.0\,s^{-1}$	k_2^-	$40.0\,s^{-1}$
k_3^+	$2000\,s^{-1}$	k_3^-	$79\,300.0\,s^{-1}\,mM^2$
k_4^+	$320.0\,s^{-1}$	k_4^-	$40.0\,s^{-1}$
Dissociation constants			
K^0_{d,Na_e}	15.5 mM	K^0_{d,Na_i}	2.49 mM
$K_{d,Ke}$	0.213 mM	$K_{d,Ki}$	0.500 mM
$K_{d,MgATP}$	2.51 mM		
Δ	−0.031		
[MgATP]	4.99 mM	[MgADP]	0.06 mM
[Pi]	4.95 mM	$[H^+]$	1000×10^{-pH} mM
pH	7.09		

The whole-cell pump flux density is given by

$$J_{NaK} = \alpha_{NaK} v_{NaK},$$

where α_{NaK} is the density of the $Na^+-K^+-ATPase$.

2.4. $Na^+-K^+-2Cl^-$ cotransporter

The major Cl^- uptake pathway is by an electroneutral $Na^+-K^+-2Cl^-$ cotransporter located in the basolateral membrane. Lytle and McManus (1986) proposed a 10-state scheme for the cotransporter. In this scheme, the sequence of ion binding is 'first on first off': on the outside of the cell a Na^+ binds first, then a Cl^-, followed by a K^+ and finally a second Cl^-. A conformational change occurs and the ions are released in the cell interior in the order Na^+, Cl^-, K^+ and Cl^-. Steps 1–4 are the ion binding stages. Step 5 represents the reorientation of the fully bound molecule so that the binding sites are accessible to the intracellular compartment. At steps 6–9, the ions are released. The unloaded cotransporter is then reorientated to the cell exterior in step 10. Benjamin and Johnson (1997) gave a quantitative description of this scheme by formulating a system of differential equations and found values for the rate constants which conform to experimental data. For our purposes, we assume that the association and dissociation of ions are in quasi steady-state, which reduces the model to a 2-state model. We then use the steady-state flux given by

$$v_{NKCC} = \frac{-k_b^{full}k_b^{empty}[Cl]_i^2[K]_i[Na]_i + k_f^{full}k_f^{empty}[Cl]_e^2[K]_e[Na]_e}{DJ_{NKCC}}.$$

Details of DJ_{NKCC} are given in Appendix B. The parameter values used here were chosen from Table 4 of Benjamin and Johnson (1997) and reproduced in Table 2. The whole-cell flux is given by

$$J_{NKCC} = \alpha_{NKCC} v_{NKCC},$$

Table 2
Parameter values for the $Na^+-K^+-2Cl^-$ cotransporter, taken from Benjamin and Johnson (1997)

Rate constants			
k_f^{full}	$1406\,s^{-1}$	k_b^{full}	$4025\,s^{-1}$
k_f^{empty}	$37\,767\,s^{-1}$	k_b^{empty}	$13\,196\,s^{-1}$
Dissociation constants			
K_{Cl}	2.42 mM	K_K	234.74 mM
K_{Na}	22.38 mM		

The dissociation constants K_{ion} in Benjamin and Johnson (1997) have units of $1\,mol^{-1}$. We have converted from mol to mmol and written the dissociation constants as $mmol\,l^{-1}$.

where α_{NKCC} is the density of the $Na^+-K^+-2Cl^-$ cotransporter.

3. Transcellular water flow model

The transepithelial movement of Cl^- into the lumen drives water flow. In our model, we assume the water travels from the interstitial region into the cell and then from the cell into the lumen (right-hand panel in Fig. 1). These flows are driven by concentration gradients between the intracellular region and the interstitium, and between the lumen and the intracellular compartment.

The rate of change of the intracellular $[Cl^-]$ is given by the equation

$$\frac{d([Cl]_i w)}{dt} = -\frac{I_{Cl}}{z_{Cl}F} + 2J_{NKCC}.$$

Cl^- is lost from the cell via the Cl^- channel, J_{Cl}, and influx of Cl^- is through the $Na^+-K^+-2Cl^-$ cotransporter, J_{NKCC}. The factor of 2 is included because the cotransporter moves 2 Cl^- ions for every K^+ and Na^+. The variable w represents the cell volume.

The rate of change of intracellular $[Na^+]$ is given by

$$\frac{d([Na]_i w)}{dt} = -3J_{NaK} + J_{NKCC}.$$

Intracellular Na^+ is pumped out of the cell by the $Na^+-K^+-ATPase$, J_{NaK}. Influx of Na^+ into the cell is via the cotransporter.

In the case of intracellular $[K^+]$, K^+ leaves the cell via K^+-channels and enters the cell via the $Na^+-K^+-ATPase$ and cotransporter. The valence of K^+ is given by z_K and is equal to +1. The rate of change of $[K^+]$ is described by

$$\frac{d([K]_i w)}{dt} = 2J_{NaK} + J_{NKCC} - \frac{I_K}{z_K F}.$$

Water flow is mediated by the increase of $[Cl^-]$ in the lumen. Fig. 2 shows a diagram for the influx of water and Cl^- into the lumen. Cl^- enters the lumen via the Ca^{2+}-activated Cl^- channel and is removed at the rate at which water leaves the cell, which we have assumed to be the same as the rate at which water enters the lumen, q_a. The lumen is modelled as a single compartment with fixed volume, w_L.

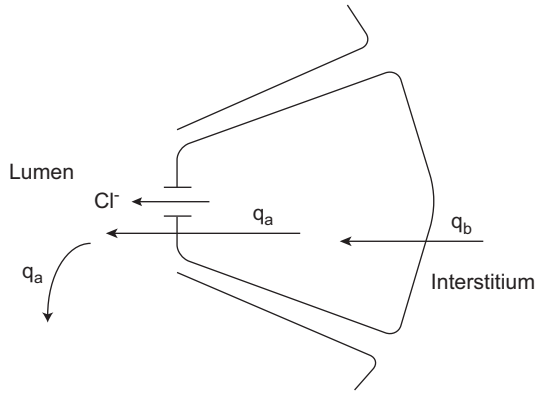

Fig. 2. Diagram showing the entry of Cl^- and water into the lumen. Water flow rates through the cell into the lumen and from the intracellular space into the cell are given by q_a and q_b, respectively.

Assuming that there is no pressure buildup, the outflow from the lumen must equal the net inflow. Hence, the rate at which water leaves the lumen is q_a. The equation for the rate of change of luminal $[Cl^-]$ is

$$w_L \frac{d[Cl]_l}{dt} = \frac{I_{Cl}}{z_{Cl}F} - q_a[Cl]_l.$$

It is experimentally observed that the cell volume shrinks upon stimulation (Foskett, 1990). Therefore we include an equation for the rate of change in the cell volume, w. The change in cell volume is determined by the differences between the intracellular, luminal and extracellular solute concentrations. As solute exits the cell upon stimulation, the cell must shrink. Equations describing the cell volume changes are

$$\frac{dw}{dt} = q_b - q_a,$$

$$q_a = RTL_{p_a}\Big([Cl]_l + [Na]_l + [K]_l - \Big([Cl]_i + [Na]_i + [K]_i + [Ca]_i + \frac{x}{w}\Big)\Big),$$

$$q_b = RTL_{p_b}\Big([Cl]_i + [Na]_i + [K]_i + [Ca]_i + \frac{x}{w} - ([Cl]_e + [Na]_e + [K]_e)\Big).$$

The water flow through the apical membrane, from the cell interior to the lumen is calculated from q_a, which describes the ionic concentration gradient between the cell and the lumen. We assume that the luminal potassium concentration $[K]_l$ is equal to the interstitial potassium concentration, $[K]_e$. Thus electroneutrality between the lumen and the interstitium is maintained by the amount of NaCl. The luminal Na^+ concentration is modified by an amount entering the lumen to maintain electroneutrality: $[Na]_l = (1/z_{Na})(z_{Na}[Na]_e + z_{Cl}[Cl]_e - z_{Cl}[Cl]_l$. The valences are $z_{Na} = +1$ and $z_{Cl} = -1$. The number of impermeable ions with units of millimoles is denoted by x. The water flow through the basolateral membrane, from the interstitium into the cell is given by q_b, which describes the concentration gradient between the intracellular space and the interstitium. Water flows from a region of high water concentration to a region of lower water concentration.

Because the surface area of the apical membrane is approximately 5% of the total surface area of the plasma membrane (Cook and Young, 1989b), this membrane will provide the main resistance to transcellular water flow. The pyramidal shape of the acinar cells also means that there is a small area for the luminal membrane and the tight junction. Therefore, there must be a relatively high water permeability regardless of whichever route the water takes (Turner and Sugiya, 2002). The large water permeability has been attributed to the presence of high concentrations of aquaporins, specifically the isoform AQP5, located in the apical membranes of many secretory epithelia, including salivary acinar cells (Raina et al., 1995). Experiments have shown that the stimulated salivary flows are reduced by greater than 60% in AQP5 knockout mice relative to normal controls (Ma et al., 1999). Therefore it appears that most of the secreted water flows through acinar cells (Turner and Sugiya, 2002). In our model, the parameter L_{p_a} is a combination of the apical water permeability and the apical surface area. Similarly, L_{p_b} is a combination of the basolateral water permeability and the basolateral surface area.

The membrane potential V_m is calculated from

$$C_m \frac{dV_m}{dt} = -I_{Cl} - I_K - FJ_{NaK} - 2FJ_{pm} + 2FJ_{in},$$

where J_{pm} and J_{in} are transmembrane Ca^{2+} fluxes, defined in the following section. We do not distinguish between an apical and basolateral membrane potential. Measurements of the basolateral membrane potential have been done in salivary acinar cells. However, the luminal membrane is not as easily accessible and so recordings of the potential across this membrane are unavailable. The electrical properties of the basolateral membrane reflect the properties of the cell as the resistance within the cell is small and the paracellular resistance is small so as to allow coupling of the electrical events at the basolateral and apical membranes (Nauntofte, 1992). Therefore we have chosen not to distinguish between the two membrane potentials.

Parameter values used in the model are given in Table 3.

Both the chloride and potassium channels are calcium dependent, so in the next section we describe a model governing the intracellular $[Ca^{2+}]$ changes.

4. Ca^{2+} model

In this section we describe a mathematical model for the changes in intracellular $[Ca^{2+}]$, based on the model developed by Sneyd et al. (2003). A schematic diagram of a cell is shown in Fig. 3.

Increase in the cytoplasmic Ca^{2+} concentration can be due, in part, to release of Ca^{2+} from internal stores such as

Table 3
Parameter values for Eqs. (4)–(11)

Maximum whole-cell conductance	
g_{cl}	31.4 nS
g_k	11.58 nS
Pump densities	
α_{NaK}	2.335×10^{-14} mmol
α_{NKCC}	4.643×10^{-14} mmol
Volume	
w_0	10^{-12} l
w_L/w_0	0.02
Water permeabilities	
L_{p_a}	1.24625×10^{-9} cm^3 (s atm)$^{-1}$
L_{p_b}	4.985×10^{-9} cm^3 (s atm)$^{-1}$
Cell capacitance	
C_m	10^{-11} F
x/w_0	55.024 mM

The resting cell volume is given by w_0 and the lumen volume is given by w_L. The lumen volume remains fixed. Parameter values were chosen to give correct steady-state solutions and behaviour.

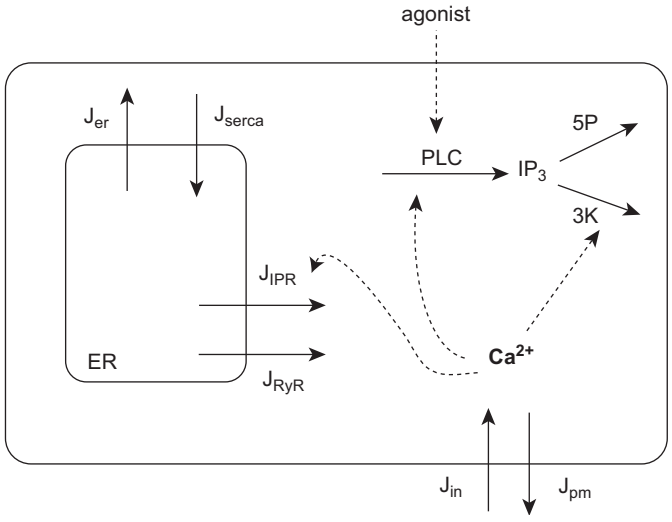

Fig. 3. Schematic of the [Ca^{2+}] model. This model includes one internal store, the endoplasmic reticulum (ER). Ca^{2+} is released from the ER via two receptors, J_{IPR} and J_{RyR} and through a passive leak, J_{er}. Ca^{2+} is then pumped back into the ER by the SERCA pump, J_{serca}. Ca^{2+} also enters the cell through an agonist-controlled influx, J_{in} and is removed by the pump J_{pm}. Ca^{2+} can also have a feedback effect (dashed lines) on various mechanisms in the cell.

the endoplasmic reticulum (ER). This release is through two types of Ca^{2+} channels: the ryanodine receptor and the inositol (1,4,5)-trisphosphate receptor (IP_3R). The IP_3R is sensitive to the second messenger IP_3. The binding of an extracellular agonist such as a hormone or neurotransmitter to a receptor in the surface membrane can cause the cleavage of phosphotidylinositol (4,5)-bisphosphate into diacylglycerol and IP_3. The IP_3 is then able to diffuse through the cell cytoplasm and bind to IP_3 receptors causing the subsequent release of Ca^{2+} from the ER.

We describe each of the mechanisms shown in Fig. 3 in the following sections.

4.1. Ca^{2+} feedback on IP_3 metabolism and IP_3 receptors

Two basic feedback mechanisms which give rise to [Ca^{2+}] oscillations in non-excitable cells have been studied (Berridge and Galione, 1988; Tsien and Tsien, 1990). The first assumes that the oscillations arise from the kinetics of the inositol (1,4,5)-trisphosphate receptor (IP_3R). In this, Ca^{2+} exerts positive and negative feedback on IP_3 receptors. On a fast time scale, Ca^{2+} can bind to the IP_3 receptor to activate it and increase its open probability; this forms a positive feedback loop. However, on a slower time scale, Ca^{2+} can bind to the IP_3 receptor at a different binding site and decrease its open probability, thus forming a negative feedback loop. In this mechanism, time-dependent IP_3 receptor gating by Ca^{2+} is crucial for generating oscillations. In the second feedback mechanism, Ca^{2+} exerts both positive and negative feedback on the production and degradation of IP_3. In positive feedback, Ca^{2+} can activate phospholipase C (PLC), leading to formation ofIP_3. The removal of IP_3 is through phosphorylation or dephosphorylation through IP_3 3-kinase (IP_3K) or IP_3 5-phosphatase (IP_3P), respectively. The removal of IP_3 by IP_3K is activated by Ca^{2+}. Such Ca^{2+}-dependent IP_3 metabolism gives rise to sustained [Ca^{2+}] oscillations.

Recently, Sneyd et al. (2006) proposed an experimental method to distinguish between the two classes of oscillatory mechanisms. They studied 13 different models, with either of the two oscillatory mechanisms. The response of each model was then tested by using a pulse of IP_3 applied to a cell exhibiting agonist-induced oscillations. Different qualitative behaviour was found for the two mechanisms. The theoretical predictions were then tested in two different cell types: pancreatic acinar cells and airway smooth muscle. It was found that in pancreatic acinar cells, Ca^{2+}-dependent IP_3 metabolism drives the Ca^{2+} oscillations. This type of experiment used to distinguish between the two types of oscillatory mechanisms has not yet been performed in parotid acinar cells, but the similarity of parotid acinar cells to pancreatic acinar cells suggests that the [Ca^{2+}] oscillations are a result of the Ca^{2+} feedback on the IP_3 metabolism. While the experiments of Sneyd et al. (2006) could distinguish between the two classes of mechanisms, they are unable to determine whether Ca^{2+} is acting on the production or degradation of IP_3. Politi et al. (2006) studied this theoretically and experimentally, on Chinese hamster ovary cells, and found that different qualitative behaviour would be observed depending on whether Ca^{2+} affected the production or degradation of IP_3. This type of experiment has not been performed in parotid acinar cells, so we include only Ca^{2+} feedback on the production of IP_3, while the removal of IP_3 is at a constant rate. The form of this equation is taken from De

Young and Keizer (1992):

$$\frac{d([IP_3]w)}{dt} = J_{IP3prod} - J_{IP3deg}, \quad (1)$$

where

$$J_{IP3prod} = \frac{w_0}{\tau_p}\left(v\frac{[Ca]_i + (1-\alpha)k_4}{[Ca]_i + k_4}\right),$$
$$J_{IP3deg} = \frac{w_0}{\tau_p}\beta[IP_3].$$

The maximum rate of IP_3 production is given by v and β is the rate constant for loss of IP_3. The parameter k_4 is the dissociation constant for Ca^{2+} stimulation of IP_3 production. We will use v as a control parameter to fit experimental data on $[Ca^{2+}]$ oscillations in parotid acinar cells.

When $\alpha = 0$, there is no Ca^{2+} feedback on the production of IP_3 and the concentration of IP_3 relaxes to a stable steady-state given by $[IP_3] = v/\beta$. Domijan et al. (2006) performed a bifurcation study in which they interpolated between the two oscillatory mechanisms by varying α. They found that for $\alpha = 0$, no oscillations are present.

4.2. The IP_3 and Ryanodine receptor models

We include $[Ca^{2+}]$ flux into the cytoplasm from the ER via the Ryanodine receptor (RyR) as well as the IP_3 receptor. The RyR is sensitive to the plant alkaloid ryanodine and is found mainly in skeletal and cardiac muscle cells and is gated by elevations of cytoplasmic Ca^{2+}. Expression of RyR in salivary acinar cells has also been shown, though the precise role of the RyR in generation of Ca^{2+} signals is not well understood (Melvin et al., 2005). We give the mathematical models for each of the two receptors below.

The IP_3 receptor model is based on the Atri et al. (1993) model. The steady-state open probability of the IP_3 receptor is a biphasic function and is given by

$$P_{IPR} = \left(\mu_0 + \frac{\mu_1[IP_3]}{k_\mu + [IP_3]}\right)\left(1 - \frac{[Ca]_i^2}{k_2^2 + [Ca]_i^2}\right)\left(b + \frac{V_1[Ca]_i}{k_1 + 1}\right),$$

where the first and third terms give the activation of the receptor by IP_3 and Ca^{2+}, respectively, and the second term describes the inactivation of the receptor. The third term is represented by a Hill function plus a leak term, which accounts for the rising part of the bell-shaped open probability curve (Atri et al., 1993). Both activation and inactivation of the receptor are fast and the open probability of the receptor follows the steady-state curve with no lag due to the speed of binding. For a complete description of the model and parameters, see Atri et al. (1993). If there is no Ca^{2+} dependence in Eq. (1) ($\alpha = 0$), then the receptor dynamics do not produce any oscillatory behaviour. The flux through the IP_3 receptor is given by

$$J_{IPR} = w_0 k_{IPR} P_{IPR}([Ca]_{er} - [Ca]_i).$$

We use a RyR model developed by Keizer and Levine (1996) for cardiac cells. In their model, it is assumed that the RyR exists in one of four states, two open (O_1 and O_2) and two closed (C_1 and C_2). By assuming that the transitions $O_1 \to C_1$ and $O_1 \to O_2$ are fast, they showed that the open probability can be expressed in the form

$$P_{RyR} = \frac{w^\infty(1 + ([Ca]_i/K_b)^3)}{1 + (K_a/[Ca]_i)^4 + ([Ca]_i/K_b)^3},$$

where

$$w^\infty(c) = \frac{1 + (K_a/[Ca]_i)^4 + ([Ca]_i/K_b)^3}{1 + 1/K_c + (K_a/[Ca]_i)^4 + ([Ca]_i/K_b)^3}.$$

The flux through the IP_3 receptor is given by

$$J_{RyR} = w_0 k_{RyR} P_{RyR}([Ca]_{er} - [Ca]_i).$$

4.3. Whole cell model

We also include a passive leak of Ca^{2+} from the ER, given by

$$J_{er} = w_0 k_{er}([Ca]_{er} - [Ca]_i).$$

The removal of Ca^{2+} back into the ER is via a SERCA pump of the form

$$J_{serca} = \frac{V_{serca}[Ca]_i}{K_{serca} + [Ca]_i}.$$

Intracellular Ca^{2+} is also modified by the entry and efflux of Ca^{2+} between the cytoplasm and the cell exterior. The entry of Ca^{2+} from the outside is an increasing function of the maximum rate of IP_3 production:

$$J_{in} = \alpha_1 + w_0\alpha_2 v/\beta.$$

The necessity that the flux J_{in} must be an increasing function of the agonist concentration was recognised theoretically by Dupont and Goldbeter (1993). We assume the agonist is linearly related to $[IP_3]$ and therefore to the rate of production. We do not make any assumptions as to the mechanism of this increase, whether by an arachidonic acid pathway (Mignen et al., 2005; Shuttleworth et al., 2004) or via capacitative entry (Berridge, 1995). Therefore we merely model the effect, which is that the flux is an increasing function of the IP_3 production rate, v. The extrusion of Ca^{2+} from the cell is maintained by the plasma membrane pump which is modelled by

$$J_{pm} = \frac{V_{pm}[Ca]_i^2}{K_{pm}^2 + [Ca]_i^2}.$$

Incorporating these terms with the receptor terms, the equations for the rates of change in intracellular $[Ca^{2+}]$ and

ER $[Ca^{2+}]$ ($[Ca^{2+}]_{er}$) are given by

$$\frac{d([Ca]_i w)}{dt} = J_{IPR} + J_{RyR} + J_{er} - J_{serca} + J_{in} - J_{pm}, \quad (2)$$

$$w_{er}\frac{d([Ca]_{er})}{dt} = -(J_{IPR} + J_{RyR} + J_{er} - J_{serca}), \quad (3)$$

Table 4
Parameter values for the Ca^{2+} model

Transport parameters			
k_{er}	$5.68 \times 10^{-3}\,s^{-1}$		
α_1	$2.4 \times 10^{-14}\,\mu mol\,s^{-1}$	α_2	$4.9984 \times 10^{-3}\,s^{-1}$
V_{serca}	$5.68 \times 10^{-11}\,\mu mol\,s^{-1}$	K_{serca}	$0.06\,\mu M$
V_{pm}	$6.816 \times 10^{-13}\,\mu mol\,s^{-1}$	K_{pm}	$0.3\,\mu M$
γ	5.405		
IP_3 parameters			
k_4	$1.07\,\mu M$	α	0.99
β	$0.50\,s^{-1}$	τ_p	1/2.84
Receptor densities			
k_{IPR}	$5.112\,s^{-1}$	k_{RyR}	$0.2272\,s^{-1}$
IP_3 R parameters			
μ_0	0.467	μ_1	0.164
k_μ	$1.61\,\mu M$	b	0.111[a]
V_1	0.889[a]	k_1	$2.1\,\mu M$[a]
k_2	$0.7\,\mu M$[a]		
RyR parameters[b]			
k_a^+	$1500\,(\mu M)^4\,s^{-1}$	k_a^-	$28.8\,s^{-1}$
k_b^+	$1500\,(\mu M)^3\,s^{-1}$	k_b^-	$385.9\,s^{-1}$
k_c^+	$1.75\,s^{-1}$	k_c^-	$0.1\,s^{-1}$

IP_3R parameters labelled with a superscript (a) are the same as those in Atri et al. (1993). RyR parameters (superscript (b)) are the same as in Keizer and Levine (1996). All other parameters have been modified to produce the correct qualitative behaviour.

where the densities of the IP_3R and the RyR are given by k_{IPR} and k_{RyR}, respectively. The ER volume is denoted by w_{er} and assumed to be fixed. The three fluxes into the cytoplasm from the ER are proportional to the difference in the Ca^{2+} concentration in the ER and the cytoplasm. Eqs. (1)–(3) make up the Ca^{2+} model.

Parameter values for the model were chosen to produce qualitatively similar behaviour to experimental results; these are given in Table 4. At steady-state, ($v = 0\,\mu M\,s^{-1}$), the resting $[Ca]_i$ is $0.05\,\mu M$ and the $[IP_3]$ is $0\,\mu M$.

4.4. Calcium buffering

Calcium buffering is included implicitly in the model. All calcium fluxes are treated as explicit fluxes, which assumes the buffers are fast, immobile and unsaturated (Wagner and Keizer, 1994; Sneyd et al., 1998).

4.5. Comparison to experimental data

We first non-dimensionalised the cell volume and the ER volume to give

$$w = w_0\bar{w}, \quad w_{er} = \frac{w_0}{\gamma},$$

where $\bar{w}$ is the non-dimensional volume and γ is the ratio of the steady-state cell volume to ER volume. The Ca^{2+} model was solved numerically, using the MatLab function `ode15s`, for various values of v to obtain qualitatively similar behaviour to the experimental Ca^{2+} traces obtained from parotid acinar cells. Ca^{2+} responses were obtained by varying concentrations of carbachol (CCh). Fig. 4A gives the experimental Ca^{2+} behaviour at three agonist

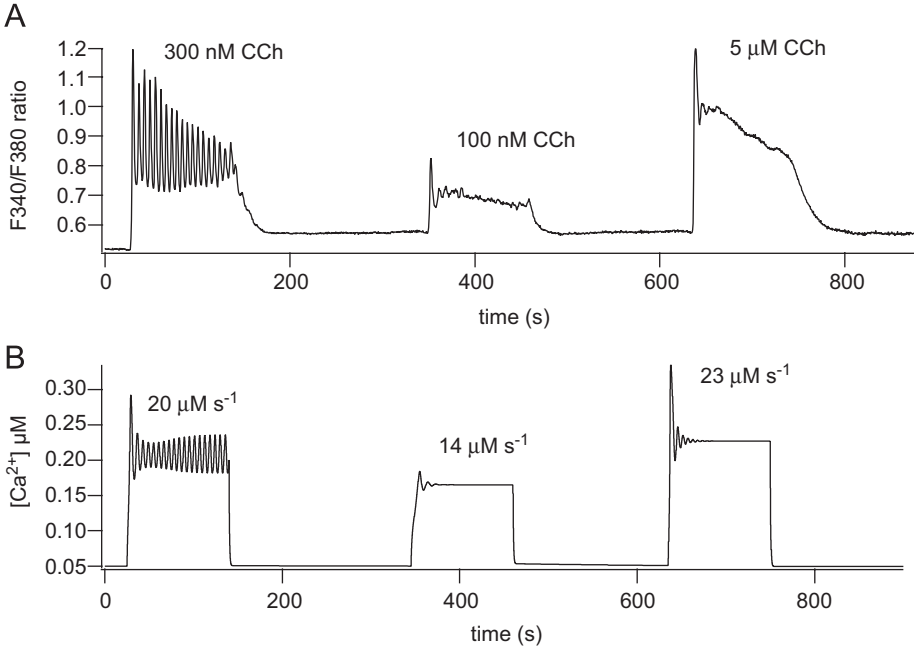

Fig. 4. (A) Experimental Ca^{2+} trace with responses using three different agonist concentrations. (B) Model behaviour. Values of v, (20, 14 and $23\,\mu M\,s^{-1}$) were chosen to give qualitatively similar behaviour to the experimental data.

concentrations and the corresponding model behaviour at three v values is shown in Fig. 4B. The experimental data show that at a medium agonist concentration, $[Ca^{2+}]$ oscillations occur. At stimulation, the $[Ca^{2+}]$ increases to a peak before decaying to oscillations on a raised base. Our model displays this behaviour: an increase to a maximum $[Ca^{2+}]$ before settling down into a regular oscillatory behaviour. At low and high agonist concentrations, the cell displays a peak of calcium, before decaying and settling to a raised steady level. Again, this experimental behaviour is reproduced by our model.

For a description of the experimental procedures used to obtain the Ca^{2+} traces, see Bruce et al. (2002).

5. Summary of model

The system of equations we solve is Eqs. (1)–(3) from the Ca^{2+} model and the following eight equations:

$$\frac{d([Cl]_i w)}{dt} = -\frac{I_{Cl}}{z_{Cl}F} + 2\alpha_{NKCC}J_{NKCC}, \tag{4}$$

$$\frac{d([Na]_i w)}{dt} = -3\alpha_{NaK}J_{NaK} + \alpha_{NKCC}J_{NKCC}, \tag{5}$$

$$\frac{d([K]_i w)}{dt} = 2\alpha_{NaK}J_{NaK} + \alpha_{NKCC}J_{NKCC} - \frac{I_K}{z_K F}, \tag{6}$$

$$w_L \frac{d[Cl]_l}{dt} = \frac{I_{Cl}}{z_{Cl}F} - q_a[Cl]_l, \tag{7}$$

$$\frac{dw}{dt} = q_b - q_a, \tag{8}$$

$$q_a = RTL_{p_a}\Big([Cl]_l + [Na]_l + [K]_l - \Big([Cl]_i + [Na]_i + [K]_i + [Ca]_i + \frac{x}{w}\Big)\Big), \tag{9}$$

$$q_b = RTL_{p_b}\Big([Cl]_i + [Na]_i + [K]_i + [Ca]_i + \frac{x}{w} - ([Cl]_e + [Na]_e + [K]_e)\Big), \tag{10}$$

$$C_m \frac{dV_m}{dt} = -I_{Cl} - I_K - FJ_{NaK} - 2FJ_{pm} + 2FJ_{in}. \tag{11}$$

6. Steady-state model

There are a number of steady-state constraints which must be taken into consideration. These include setting the resting intracellular ion concentrations and the membrane potential at physiologically reasonable values. Experimentally, the open probability of the Ca^{2+}-activated Cl^- and K^+ channels is low at steady-state (Arreola et al., 1996; Takahata et al., 2003), so there is very little current flow. We have chosen parameters to give correct steady-state behaviour when the rate of IP_3 production, v, is zero. At zero rate of production, the IP_3 concentration is 0 μM and the $[Ca^{2+}]$ 0.05 μM. In solving the equations, we non-dimensionalised the variable cell volume by the resting cell volume, w_0.

Table 5
Steady-state concentrations, resting potential and apical flow rate at zero IP_3 production rate

$[Cl]_i$	60.00 mM	$[Na]_i$	15.00 mM
$[K]_i$	140.00 mM	$[Cl]_l$	115.05 mM
V_m	−60.01 mV		
w	10^{-12} l	q_a/w_0	0.002549 s^{-1}

The apical flow rate has been normalised by resting cell volume, w_0.

The steady-state ion concentrations, membrane potential and cell volume are given in Table 5.

The $[Cl]_i$ is 60 mM, which agrees well with the 61 mM in Foskett (1990). The $[Cl]_i$ is also affected by the efflux of Cl^- via the Cl^- channel. At low $[Ca]_i$, the open probability of the channel is low. The current through the Cl^- channel when $[Ca]_i = 0.05$ μM and $V_m = -60$ mV is −0.001056 nA. At steady-state, the efflux of Cl^- through the Cl^- channel must be balanced by the influx via the $Na^+-K^+-2Cl^-$ cotransporter. According to Foskett (1990), the high $[Cl^-]$ under unstimulated conditions is maintained by the cotransporter. Parameter values were chosen so that the intracellular $[Cl^-]$ is 60 mM. The K^+ channel is Ca^{2+} dependent and at low $[Ca]_i$, there is very little K^+ efflux through this channel. Intracellular K^+ concentration is maintained by the influx of K^+ via the $Na^+-K^+-2Cl^-$ cotransporter and the Na^+-K^+-ATPase.

We note that the normalised flow rate, q_a/w_0, is not zero at steady state, but this is not unexpected. Under normal conditions, salivary glands maintain a low level of saliva flow.

The resting membrane potential has been found to vary from −20 to −70 mV and in mouse and rat salivary acinar cells, the membrane potential is in the range of −55 to −70 mV (Nauntofte, 1992). Romanenko et al. (2006) found experimentally the resting potential of parotid acinar cells in wild-type mice was near −60 mV. Our model gives a steady-state membrane potential of −60.01 mV.

At steady-state, the ionic composition of the lumen is similar to ionic concentrations in the interstitium, where $[Cl]_e = 115$ mM, $[Na]_e = 150$ mM and $[K]_e = 5$ mM. Thus in our model the ionic composition of the primary secretion reflects the Cl^-, Na^+ and K^+ concentrations in the interstitium (Melvin et al., 2005). The choice of the water permeabilities ensured that this condition was satisfied.

7. Model results

7.1. A solution

To obtain a stimulated water flow, we solved Eqs. (4)–(11) and the Ca^{2+} model with the rate of IP_3 production, v, set at 20 μM s^{-1}. At this value of v, the Ca^{2+} system is in an oscillatory mode, as can be seen in Fig. 4B. Fig. 5 shows the corresponding oscillatory behaviour exhibited in the water flow system. This oscillatory behaviour is a result of the Ca^{2+}-dependence

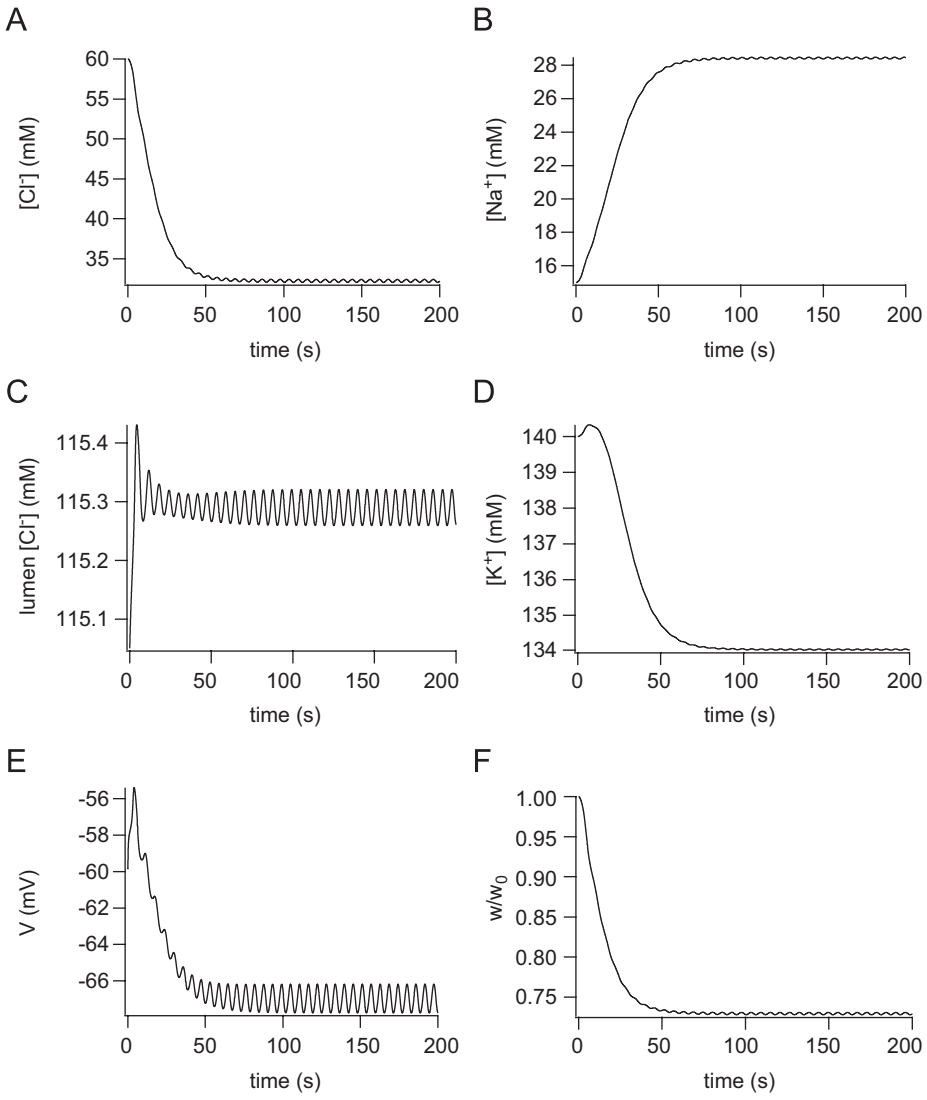

Fig. 5. Oscillations in the Cl^-, Na^+, luminal Cl^-, K^+ concentrations (panels A–D, respectively), as well as the membrane potential, V_m (panel E), and the normalised cell volume, w/w_0 (panel F).

of the Cl^- and K^+ channels. Again, the variable cell volume has been non-dimensionalised by w_0.

Upon stimulation, ($v = 20\,\mu M\,s^{-1}$), the Cl^- concentration drops by approximately 50%, (see Fig. 5A), which agrees with the experimental data of Foskett (1990) in which the Cl^- concentration fell to approximately 33 mM from a resting level of 61 mM. The $[K^+]_i$ also drops as a result of the activation of the K^+ channels. Both the luminal $[Cl^-]$ and intracellular $[Na^+]$ increase. The model also shows that the cell volume decreases by approximately 27% which is slightly higher than the 15–20% decrease found by Foskett and Melvin (1989). The sustained cell shrinkage during sustained elevated $[Ca^{2+}]$ reflecting sustained fluid secretion (Foskett and Melvin, 1989) can be seen in the model. An elevated average $[Ca^{2+}]$ over the entire oscillatory period causes a sustained average cell shrinkage (Fig. 5F) and sustained average raised fluid secretion rate (Fig. 6A). The average normalised water flow rate is $0.01380\,s^{-1}$, which is 5.4 times the resting rate.

Fig. 6 shows the oscillating water flow rate (panel A) and the luminal and intracellular solute concentrations (panel B), which generate this flow. In panel B, the top curve shows the luminal solute concentration and the bottom curve shows the intracellular solute concentration. The solute concentration in the interstitium is fixed at 270 mM. As can be seen, the luminal solute concentration is similar to interstitial solute concentration. Even though the luminal solute concentration is nearly isotonic to that in the intracellular space, an increased water flow q_a rate into the lumen is generated.

The coupling of cell volume to intracellular $[Ca^{2+}]$ was considered by Foskett and Melvin (1989) who found that shrinkage of the cell was detected close to the time that the $[Ca]_i$ reached peaked levels. They found even after the increase began to subside, the cell continued to shrink. Our model shows the cell shrinkage to occur on a much slower time scale than that of $[Ca]_i$ increase. This can be seen in Fig. 7. As the $[Ca^{2+}]$ settles into an oscillatory behaviour,

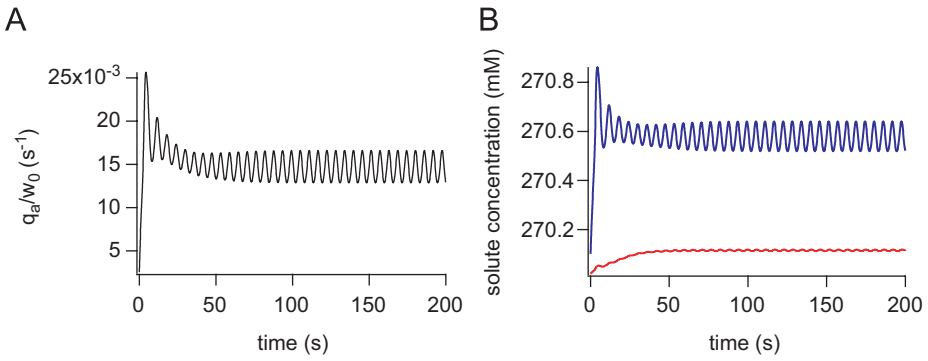

Fig. 6. Panel A shows the normalised water flow rate $\tilde{q}_a$ and B shows the total solute concentration in the lumen (upper curve) and in the intracellular space (lower curve).

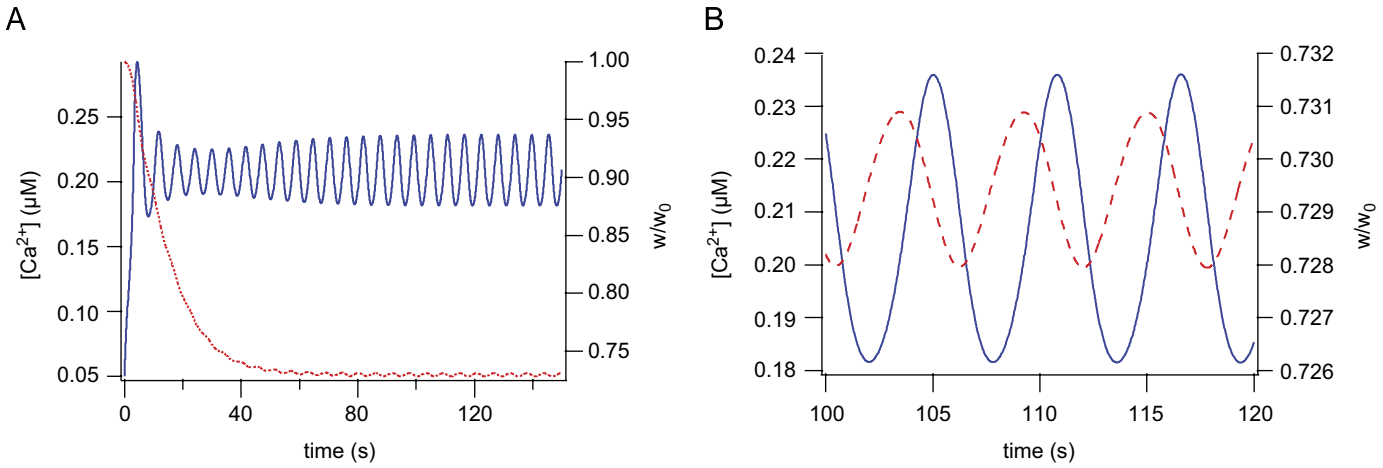

Fig. 7. (A) Oscillations in $[Ca]_i$ (left axis) and cell volume (right axis, dashed curve). (B) Close up of oscillations in $[Ca^{2+}]$ (left axis) and cell volume (right axis, dashed curve).

the cell volume still continues to shrink before reaching minimum volume after approximately 40 s. After this, the cell volume begins to oscillate at around 73% of the original cell volume, w_0. Panel B shows the oscillations in the $[Ca]_i$ and cell volume are slightly out of phase. The cell volume does not reach minimum volume when the $[Ca]_i$ peaks. Foskett and Melvin (1989) found that the minimum cell volume is reached at approximately the time when the $[Ca]_i$ reached its maximum value. We note that the magnitude of our oscillations are small and that the volume stays around 70% of the resting cell volume during stimulation. Foskett and Melvin (1989) found that the cell volume oscillates between the resting cell volume and 80% of the volume. These are associated with $[Ca^{2+}]$ oscillating between a baseline steady-state value of 0.06 μM up to 0.5 μM. The main reason for the discrepancy between our model results and the experimental findings of Foskett and Melvin (1989) occurs because our $[Ca^{2+}]$ oscillates on a raised base, above the steady-state concentration, between 0.15 and 0.25 μM. We investigated using the model of Sneyd et al. (2003), in which the $[Ca^{2+}]$ oscillated between the steady-state concentration and a maximum amplitude, and found corresponding changes to the oscillations in cell volume. The cell volume then oscillated between the resting cell volume and 80% of w_0.

A tight temporal relationship between cell volume and $[Cl]_i$ was also observed in Foskett (1990). This is clearly seen in the model results in Fig. 8. Panel A shows the oscillations in the cell volume and $[Cl]_i$ to be in phase, and this can be seen also in the phase plot in panel B in which the cell volume is plotted against the $[Cl^-]$. Initially, the cell volume and Cl^- concentration are at their steady-state values, but they then decrease.

We investigated whether the water flow rate is affected by the $[Ca]_i$ oscillation frequency or whether it is the average $[Ca]_i$ which controls the rate. Note all flow rates are normalised by the resting cell volume. Fig. 9 presents the average water flow rate, q_a, against varying v, frequency and average $[Ca]_i$. Panel A shows $[Ca]_i$ oscillation frequency versus v, the maximum rate of IP_3 production. Except for v between 17 and 18 μM s^{-1}, the frequency of oscillations is an increasing function of v. Panel B shows the average flow rate against v. This figure seems to indicate that an increasing flow rate is related to an increasing v and frequency. However, we then calculated the average flow rate versus frequency, shown in panel C,

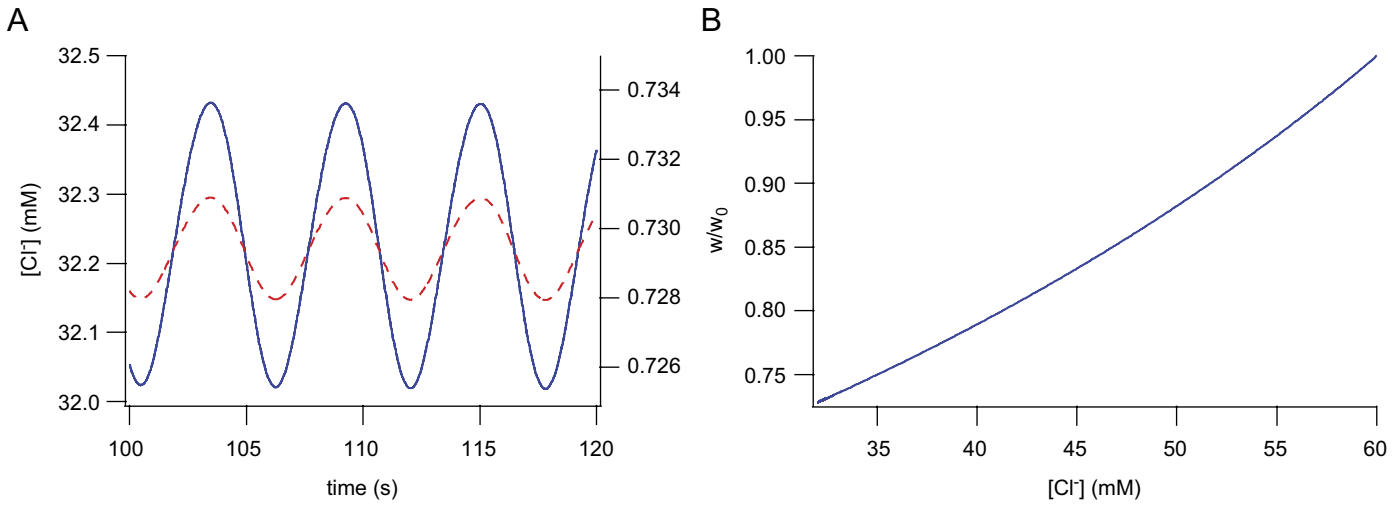

Fig. 8. Panel A shows the $[Cl^-]$ plotted on the left axis (solid curve) and the cell volume on the right axis (dashed curve), and the panel B gives the phase plot of the cell volume versus the $[Cl^-]$.

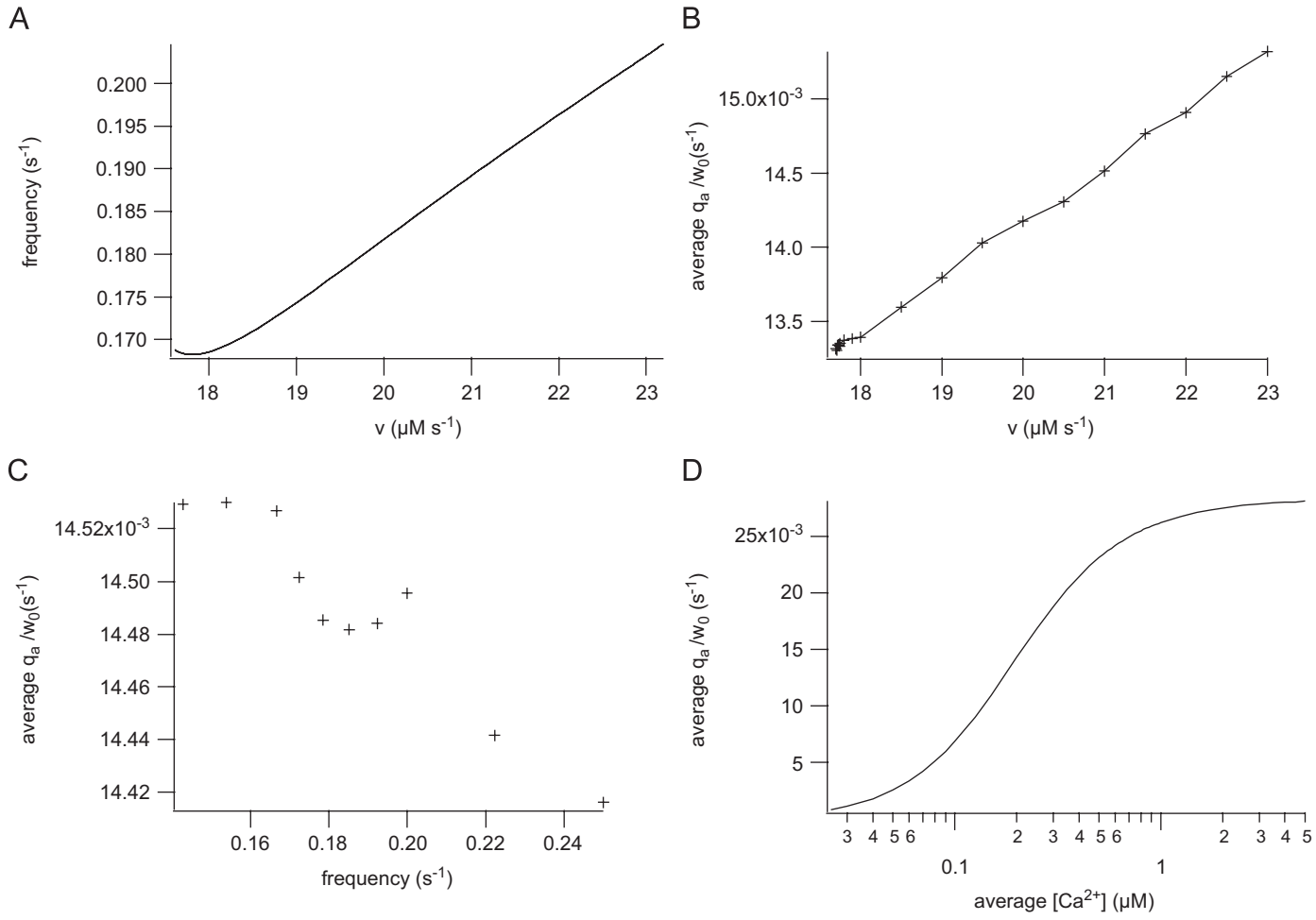

Fig. 9. (A) Frequency of $[Ca]_i$ oscillations against v. (B) Plot of the average flow rate against v. Crosses mark the v values used. (C) Average water flow for various frequencies is plotted against the average $[Ca]_i$ fixed at 0.2 μM. (D) Average flow rate against increasing average $[Ca^{2+}]$.

but kept the average $[Ca]_i$ fixed at 0.2 μM. These calculations were done by using a periodic square-wave to describe the calcium concentration. The average $[Ca]_i$ was kept fixed, while varying the maximum value of the oscillation, c_{max}, with a period of t_{max}, and the minimum value of the oscillation, c_{min}, with a period of t_{min}. The

range of variation in the flow rate is 10^{-5}, which suggests that the frequency of $[Ca]_i$ oscillations does not affect the flow rate. In panel D, we plot the average flow rate against fixed average $[Ca]_i$, showing that the change in the flow rate is mediated by the $[Ca^{2+}]$. A higher average $[Ca]_i$ causes a higher average water flow rate. As it is the average $[Ca]_i$ which affects the flow rate, the increasing trend in the flow rate in the panel B is a result of the $[Ca]_i$ at each v value.

7.2. Varying parameters

The water permeabilities for cells given in House (1974) are smaller than the values we have chosen to produce the results in the previous section. The water permeabilities were chosen to satisfy the condition that the ionic composition of the lumen is similar to the composition in the interstitium. In this section we investigate changing these parameters and the effect on our model results.

We decreased the water permeabilities by factors of 10 and 100. The results are plotted in Fig. 10. Decreasing the water permeability by a factor of 10 does not affect the results qualitatively and has very little effect quantitatively on the water flow. However, the difference between the luminal and intracellular solute concentrations has increased by 10 from the difference resulting from using the water permeabilities given in Table 3. Decreasing the water permeabilities by a factor of 100 has no qualitative effect, but quantitatively the water flow has decreased and the difference between the luminal and intracellular solute concentrations has increased. By using a smaller water permeability, there is more resistance, and thus there needs to be a greater driving force, given by a greater difference between the luminal and intracellular solute concentrations. This can be seen in Fig. 10D.

Parameter values for the whole cell chloride and potassium conductances, g_{Cl} and g_K, were found experimentally, but the $Na^+-K^+-2Cl^-$ and Na^+-K^+-ATPase densities were chosen to give correct steady-state values. Here we vary the values of α_{NKCC} and α_{NaK} by $\pm 10\%$ and look at how the steady-state values were affected. Steady-state values are shown in Table 6. Only small quantitative differences occur in the steady-state values.

8. Discussion

Salivary fluid secretion is crucial for many essential functions. These include protection of teeth, providing an antibacterial action and mastication. Individuals with a reduced salivary flow experience a range of complaints

Table 6
Steady-state $[Cl]_i$, resting potential and normalised cell volume

	$[Cl]_i$	V_m	w
$(\alpha_{NKCC}, \alpha_{NaK})$	60.0057	−60.0041	1.0000
$(\alpha_{NKCC} - 10\%, \alpha_{NaK})$	59.2551	−60.2335	0.9901
$(\alpha_{NKCC} + 10\%, \alpha_{NaK})$	60.6476	−59.8091	1.0086
$(\alpha_{NKCC} - 10\%, \alpha_{NaK} - 10\%)$	58.5023	−60.3821	0.9804
$(\alpha_{NKCC} + 10\%, \alpha_{NaK} + 10\%)$	61.3727	−59.6636	1.0186

The first row uses the densities given in Table 3, and is given as a reference. All other model parameters are unchanged.

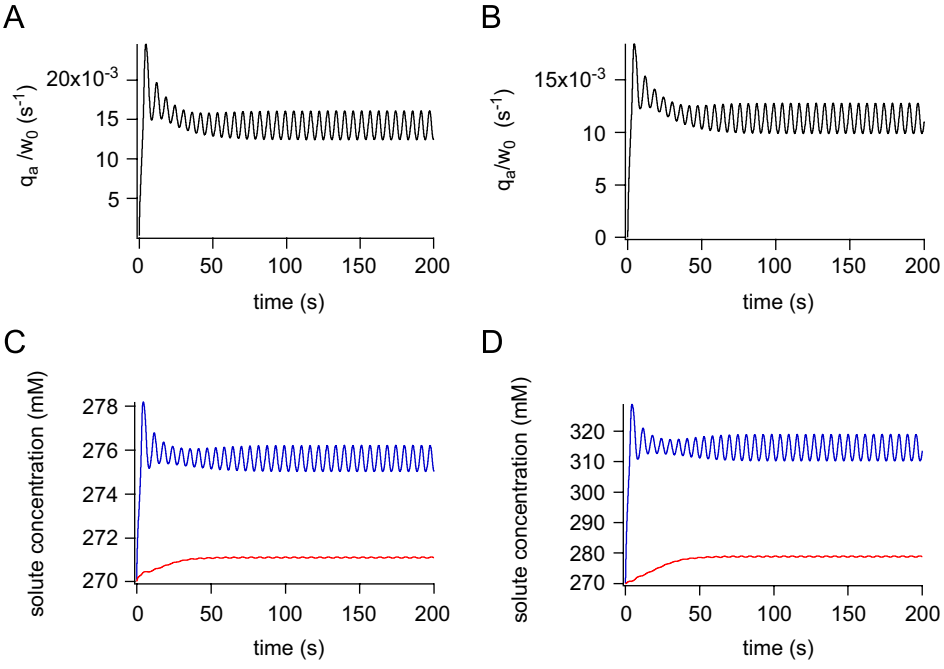

Fig. 10. The first column gives the results using water permeabilities 10 times less than used in the previous section, while the second column uses water permeabilities 100 times less than in the previous section. The normalised water flow and luminal and intracellular solute concentrations are plotted. In panels C and D, the top curve shows the luminal solute concentration and the lower curve shows the intracellular solute concentration.

such as a feeling of dryness, alterations in taste, difficulty in chewing, swallowing and speaking.

We have constructed a mathematical model for the mechanisms underlying salivary fluid secretion in a parotid acinar cell. The model is based on a physiological model shown in Fig. 1. We first constructed a model to describe the channels and transporters whose concerted actions generate water flow. This model gave correct steady-state behaviour in the ion concentrations, membrane potential and currents. We then developed a Ca^{2+} model describing intracellular [Ca^{2+}] oscillations. The model parameters were chosen to give qualitative agreement with the experimental traces. As can be seen in Fig. 4, our model gives good qualitative agreement with the data. We also used another set of experimental data from mouse parotid acinar cells and found that our model parameters also fit the second set of data.

Our Ca^{2+} model includes feedback on the production of IP_3. Experimentally it is possible to distinguish between whether it is Ca^{2+} feedback on the IP_3 receptors or on IP_3 metabolism which is the main oscillatory mechanism. Sneyd et al. (2006) proposed such an experiment. They found that Ca^{2+} oscillations in pancreatic acinar cells depended on IP_3 metabolism by Ca^{2+}. Such an experiment has yet to be performed on parotid acinar cells, but the similarity of these cells to pancreatic acinar cells suggests that the same oscillatory mechanism exists.

Our salivary fluid model is based on the physiological model shown in Fig. 1, which is the current accepted model. However other models have been proposed, one which provides an alternative Cl^- uptake mechanism and another in which the secretion of HCO_3^- rather than Cl^- into the lumen controls the water flow. The first alternative modifies the Cl^- exchange process. The $Na^+-K^+-2Cl^-$ cotransporter is replaced by a Cl^-/HCO_3^- and a Na^+/H^+ exchanger. Upon stimulation, the decrease in the Cl^- concentration leads to increased Cl^- entry via the Cl^-/HCO_3^- exchanger. The HCO_3^- is replaced by diffusion of CO_2 into the cell and its conversion into HCO_3^- and H^+ by carbonic anhydrase (CA). The H^+ are then removed from the cell by the Na^+/H^+ exchanger. The second alternative involves the secretion of HCO_3^- instead of Cl^- into the lumen to drive fluid secretion. CO_2 enters the cell across the basolateral membrane and is converted to HCO_3^- and H^+ by intracellular CA. HCO_3^- is secreted across the apical membrane into the lumen and H^+ is removed by the Na^+/H^+ exchanger. In most salivary acinar cells, the paired Cl^-/HCO_3^- and Na^+/H^+ exchangers are present (Melvin et al., 2005). Evans et al. (2000) found that stimulated salivary flow rates in $Na^+-K^+-2Cl^-$ cotransporter knockout mice were only 40% of the rate observed in normal littermates, but that the activity of the Cl^-/HCO_3^- exchanger was increased in parotid acinar cells from the knockout mice. This seems to suggest that fluid secretion via the first alternative is increased to compensate for the loss of the cotransporter. We have yet to include these other transport mechanisms.

We did not distinguish between apical and basolateral membrane potentials. As mentioned, the luminal membrane accounts for 5% of the total plasma membrane and thus, accessibility of this membrane is limited and recordings of the membrane potential have not been obtained. Lang and Walz (2001) recorded the basolateral and transepithelial membrane potentials in cockroach salivary duct cells and found that upon stimulation, the basolateral potential depolarised from −65 to −31 mV and the transepithelial membrane potential hyperpolarized from −13 to −22 mV. However, no measurements have been obtained for parotid acinar cells. It has been claimed that the small paracellular resistance allows the coupling of electrical activity in the basolateral and apical membranes and as the resistance within the cell is small, the electrical properties of the basolateral membrane reflects the properties of the whole acinar cell (Nauntofte, 1992). The presence of K^+ in the primary fluid also raises the possibility that K^+ channels exist in the apical membrane. While uncaging of caged Ca^{2+} in pancreatic acinar cells has revealed the localisation of Cl^- channels in the apical membrane only (Park et al., 2001), similar experiments have not been done to establish the location of K^+ channels. Therefore the possibility of K^+ channels in the apical membrane cannot be ruled out. These K^+ channels would cause the membrane potential at the apical membrane to hyperpolarise as it does in the basolateral membrane. Cook and Young (1989a) investigate the effect of K^+ channels in the apical membrane on epithelial secretion and find that their presence can enhance fluid secretion.

Fluid flow arises from activation of Ca^{2+}-dependent Cl^- and K^+ channels by elevated [Ca^{2+}]. The $[Ca]_i$ oscillations cause oscillations in the intracellular [Cl^-] and [K^+] and thus the other variables. The features of the fluid flow model oscillations are a result of the $[Ca]_i$ oscillations. In particular, the raised bases of the [Na^+] and luminal [Cl^-] oscillations and the small amplitudes of all the oscillations in Figs. 5 and 6 are a result of the raised base of $[Ca]_i$ oscillations and the small amplitude $[Ca]_i$ oscillations, respectively. The modulation of [Cl^-], [Na^+], [K^+] and cell volume by intracellular [Ca^{2+}] has been shown experimentally by Foskett (1990), Foskett and Melvin (1989) and Wong and Foskett (1991). In measurements on rat parotid acinar cells, Wong and Foskett (1991) found larger amplitude [Na^+] oscillations than those observed in our simulations, corresponding to larger amplitude [Ca^{2+}] oscillations that they observed. The discrepancy between our $[Na]_i$ oscillations and those of Wong and Foskett (1991) is the result of differences in intracellular [Ca^{2+}] between our model simulations and those observed in their study. Our [Ca^{2+}] oscillations were fitted to experimental data obtained from mouse parotid acinar cells, which showed much lower [Ca^{2+}] amplitude than observed by Wong and Foskett (1991), and hence lower amplitude [Na^+] oscillations. Reparameterisation of our model to produce increased amplitude of [Ca^{2+}] oscillations would

have a similar knock-on effect on the magnitude of the $[Na^+]$ oscillations generated.

Our model parameters (given in Table 3) were chosen to give steady-state values in physiological ranges. The water permeabilities were chosen to satisfy the condition that the ionic composition of the lumen is similar to the composition in the interstitium. The water permeabilities for cells given in House (1974) are smaller than the values we have chosen. We found that smaller water permeabilities did not give the result of isotonicity between the lumen and interstitium. Where possible, the fluid flow model used parameters which were found from experimental data, for example, the conductances of the chloride and potassium channels. Densities of the $Na^+-K^+-ATPase$ and $Na^+-K^+-2Cl^-$ cotransporter were chosen to balance the fluxes through the chloride and potassium channels in order to give physiologically correct steady-state intracellular ion concentrations. A variation of $\pm 10\%$ in the densities did not affect the results qualitatively and had little effect quantitatively.

The oscillations in the water flow model are coupled to the $[Ca]_i$ oscillations. We found that the average flow rate is a result of the average $[Ca]_i$, with a higher average $[Ca]_i$ generating a higher average water flow rate. We showed in Fig. 9 that the average flow rate was independent of the frequency. We varied the frequency, but kept the average $[Ca]_i$ fixed and found there was no major change in the flow rate.

Evans et al. (2000) found the parotid saliva flow rate to be between 5 and 15 $\mu l\,min^{-1}$ per 100 g parotid gland and the volume of saliva secreted in 50 min is 400 μl per 100 g, in mice whose average parotid gland weights were 38.2 mg. Using their volume of saliva secreted, and assuming that one cell has volume of 1 pl and that water contributes to the entire volume of the cell, we estimate that there are a maximum of 10^8 cells per 100 g of parotid gland. The total volume secreted by one cell upon stimulation, in our model, is 4.133×10^{-5} μl in 50 min. To achieve the experimental volume of saliva, our model would require that there are 9.672×10^6 cells in 100 g. This agrees well with our estimate of a maximum of 10^8 cells.

In this paper we have presented the results for transcellular water flow. Recent experimental evidence has shown that in AQP5 knockout mice, the stimulated salivary flows are reduced by greater than 60% (Ma et al., 1999), which seems to suggest that most of the water flows through the cells. We also developed a model for paracellular water flow, in which water flow into the lumen is generated by the osmotic gradient between the luminal and interstitial solute concentrations. We used the apical membrane permeability, L_{p_a}, for the tight junction permeability. The transcellular model parameters were used, and, not surprisingly, gave the same steady-state values as for the transcellular model. We found the qualitative features of the paracellular model to be similar to the transcellular model. A full study of a combination of the two water flow routes is left to future study.

The activation of Ca^{2+}-dependent ion channels is the primary mechanism underlying salivary fluid secretion from the parotid gland (Putney, 1986), but secretion can be enhanced when both Ca^{2+} and cyclic-AMP (cAMP) signalling pathways are activated concurrently (Melvin et al., 2005). The next step in our modelling is to include the interactions between the cAMP and $[Ca^{2+}]$ signalling pathways and investigate the consequences for the shaping of $[Ca^{2+}]$ signals in parotid acinar cells. The two signalling pathways interact on multiple levels. Not only does cAMP regulate $[Ca^{2+}]$ dynamics at a number of loci, but changes in $[Ca^{2+}]$ can modulate the production of cAMP (Cooper et al., 1995). A theoretical study of these interacting pathways will require the construction and testing of a new model of $[Ca^{2+}]$ oscillations.

Our model describes water flow in an isolated parotid acinar cell. Further work includes a spatial description of the cell and modelling a parotid acinus with coupled acinar cells to determine the effect on the overall salivary fluid secretion.

Acknowledgements

We thank Ted Begenisich and James Melvin for helpful discussions. We also wish to thank the anonymous reviewer, whose careful reading of our original manuscript turned up errors which we have now corrected. The comments have improved our model and this manuscript. Elan Gin was supported by the Tertiary Education Commission's Top Achiever Doctoral Scholarship. This work was supported by National Institutes of Health (NIH) Grants R01-DE14756 and R01-DE16999.

Appendix A. $Na^+-K^+-ATPase$ details

The steady-state flux for the $Na^+-K^+-ATPase$ is given by

$$v_{NaK} = \frac{\alpha_1^+\alpha_2^+\alpha_3^+\alpha_4^+ - \alpha_1^-\alpha_2^-\alpha_3^-\alpha_4^-}{\Sigma},$$

where

$$\alpha_1^+ = \frac{k_1^+\widetilde{Na}_i^3}{(1+\widetilde{Na}_i)^3 + (1+\widetilde{K}_i)^2 - 1}, \quad \alpha_2^+ = k_2^+,$$

$$\alpha_3^+ = \frac{k_3^+\widetilde{K}_e^2}{(1+\widetilde{Na}_e)^3 + (1+\widetilde{K}_e)^2 - 1}, \quad \alpha_4^+ = \frac{k_4^+\widetilde{MgATP}}{1+\widetilde{MgATP}},$$

$$\alpha_1^- = k_1^-[MgADP], \quad \alpha_2^- = \frac{k_2^-\widetilde{Na}_e^3}{(1+\widetilde{Na}_e)^3 + (1+\widetilde{K}_e)^2 - 1},$$

$$\alpha_3^- = \frac{k_3^-[Pi][H^+]}{1+\widetilde{MgATP}}, \quad \alpha_4^- = \frac{k_4^-\widetilde{K}_i^2}{(1+\widetilde{Na}_i)^3 + (1+\widetilde{K}_i)^2 - 1},$$

where

$$\widetilde{\mathrm{Na}}_i = \frac{[\mathrm{Na}]_i}{K_{d,Na_i}}, \quad \widetilde{\mathrm{K}}_i = \frac{[\mathrm{K}]_i}{K_{d,K_i}},$$
$$\widetilde{\mathrm{Na}}_e = \frac{[\mathrm{Na}]_e}{K_{d,Na_e}}, \quad \widetilde{\mathrm{K}}_e = \frac{[\mathrm{K}]_e}{K_{d,K_e}},$$
$$\widetilde{\mathrm{MgATP}} = \frac{[\mathrm{MgATP}]}{K_{d,MgATP}}.$$

The voltage dependence is through the Na^+ dissociation reactions:

$$K_{d,Na_e} = K^0_{d,Na_e} \exp((1+\Delta)FV/3RT),$$
$$K_{d,Na_i} = K^0_{d,Na_i} \exp(\Delta FV/3RT)$$

and

$$\begin{aligned}\Sigma = {} & \alpha_1^-\alpha_2^-\alpha_3^- + \alpha_1^-\alpha_2^-\alpha_4^+ + \alpha_1^-\alpha_3^+\alpha_4^+ + \alpha_2^+\alpha_3^+\alpha_4^+ \\ & + \alpha_2^-\alpha_3^-\alpha_4^- + \alpha_1^+\alpha_2^-\alpha_3^- + \alpha_1^+\alpha_2^-\alpha_4^+ + \alpha_1^+\alpha_3^+\alpha_4^+ \\ & + \alpha_1^-\alpha_3^-\alpha_4^- + \alpha_2^+\alpha_3^-\alpha_4^- + \alpha_1^+\alpha_2^+\alpha_3^- + \alpha_1^+\alpha_2^+\alpha_4^+ \\ & + \alpha_1^-\alpha_2^-\alpha_4^- + \alpha_1^-\alpha_3^+\alpha_4^- + \alpha_2^+\alpha_3^+\alpha_4^- + \alpha_1^+\alpha_2^+\alpha_3^+.\end{aligned}$$

Details of the derivation can be found in Smith and Crampin (2004). Thermodynamic arguments give that

$$\frac{k_1^+k_2^+k_3^+k_4^+K_{d,K_i}^2K_{d,Na_e}^3}{k_1^-k_2^-k_3^-k_4^-K_{d,MgATP}K_{d,K_e}^2K_{d,Na_i}^3} = \exp(-\Delta G^0_{MgATP}/RT)\exp(FV_m/RT),$$

where ΔG^0_{MgATP} is the standard free energy. This constraint provides no information on the location of a voltage-dependent transition step. Smith and Crampin (2004) place this in the Na^+ dissociation constants.

Appendix B. $Na^+-K^+-2Cl^-$ cotransporter details

The steady-state flux is given by

$$v_{NKCC} = \frac{-k_b^{full}k_b^{empty}[\mathrm{Cl}]_i^2[\mathrm{Na}]_i[\mathrm{K}]_i + k_f^{full}k_f^{empty}[\mathrm{Cl}]_e^2[\mathrm{Na}]_e[\mathrm{K}]_e}{DJ_{NKCC}},$$

where

$$\begin{aligned}DJ_{NKCC} = {} & Z_{nkcc1} + Z_{nkcc2} + Z_{nkcc3} + Z_{nkcc4} + Z_{nkcc5} + Z_{nkcc6} \\ & + Z_{nkcc7} + Z_{nkcc8} + Z_{nkcc9} + Z_{nkcc10} + Z_{nkcc11} \\ & + Z_{nkcc12} + Z_{nkcc13} + Z_{nkcc14} + Z_{nkcc15} + Z_{nkcc16}\end{aligned}$$

and

$$Z_{nkcc1} = Z_1[\mathrm{Cl}]_i, \quad Z_{nkcc2} = Z_2[\mathrm{Na}]_e, \quad Z_{nkcc3} = Z_3[\mathrm{Cl}]_i[\mathrm{K}]_i,$$
$$Z_{nkcc4} = Z_4[\mathrm{Cl}]_e[\mathrm{K}]_e, \quad Z_{nkcc5} = Z_5[\mathrm{Cl}]_i^2[\mathrm{K}]_i,$$
$$Z_{nkcc6} = Z_6[\mathrm{Cl}]_e[\mathrm{K}]_e[\mathrm{Na}]_e, \quad Z_{nkcc7} = Z_7[\mathrm{Cl}]_i^2[\mathrm{K}]_i[\mathrm{Na}]_i,$$
$$Z_{nkcc8} = Z_8[\mathrm{Cl}]_e^2[\mathrm{K}]_e[\mathrm{Na}]_e, \quad Z_{nkcc9} = Z_9[\mathrm{Cl}]_i^2[\mathrm{K}]_i[\mathrm{Na}]_i[\mathrm{Na}]_e,$$
$$Z_{nkcc10} = Z_{10}[\mathrm{Cl}]_i[\mathrm{Cl}]_e^2[\mathrm{K}]_e[\mathrm{Na}]_e,$$
$$Z_{nkcc11} = Z_{11}[\mathrm{Cl}]_i^2[\mathrm{K}]_i[\mathrm{Na}]_i[\mathrm{Cl}]_e[\mathrm{Na}]_e,$$
$$Z_{nkcc12} = Z_{12}[\mathrm{Cl}]_i[\mathrm{K}]_i[\mathrm{Cl}]_e^2[\mathrm{K}]_e[\mathrm{Na}]_e,$$
$$Z_{nkcc13} = Z_{13}[\mathrm{Cl}]_i^2[\mathrm{K}]_i[\mathrm{Cl}]_e^2[\mathrm{K}]_e[\mathrm{Na}]_e,$$
$$Z_{nkcc14} = Z_{14}[\mathrm{Cl}]_i^2[\mathrm{K}]_i[\mathrm{Na}]_i[\mathrm{Cl}]_e[\mathrm{K}]_e[\mathrm{Na}]_e,$$
$$Z_{nkcc15} = Z_{15}[\mathrm{Cl}]_i^2[\mathrm{K}]_i[\mathrm{Na}]_i[\mathrm{Cl}]_e^2[\mathrm{K}]_e[\mathrm{Na}]_e,$$
$$Z_{nkcc16} = K_{Cl}^2K_{Na}K_K(k_b^{empty} + k_f^{empty})$$

with

$$Z_1 = K_{Cl}K_KK_{Na}k_b^{empty}, \quad Z_2 = K_{Cl}^2K_Kk_f^{empty},$$
$$Z_3 = K_{Cl}K_{Na}k_b^{empty}, \quad Z_4 = K_{Cl}K_Kk_f^{empty},$$
$$Z_5 = K_{Na}k_b^{empty}, \quad Z_6 = K_{Cl}k_f^{empty},$$
$$Z_7 = k_b^{empty} + k_b^{full}, \quad Z_8 = k_f^{full} + k_f^{empty},$$
$$Z_9 = L_{Na}k_b^{full}, \quad Z_{10} = L_{Cl}k_f^{full},$$
$$Z_{11} = L_{Cl}L_{Na}k_b^{full}, \quad Z_{12} = L_{Cl}L_Kk_f^{full},$$
$$Z_{13} = L_{Cl}^2L_Kk_b^{full}, \quad Z_{14} = L_{Cl}L_KL_{Na}k_b^{full},$$
$$Z_{15} = L_{Cl}^2L_KL_{Na}(k_b^{full} + k_f^{full}).$$

where the L_{ion} are reciprocals of the K_{ion} and have units of $\mathrm{l\,mmol^{-1}}$.

This reaction is closed thermodynamically, so the product of the equilibrium constants must equal one. This was taken into consideration by Benjamin and Johnson (1997) who calculated the arbitrarily chosen rate constant, k_b^{empty}, from the remaining rate constants:

$$k_b^{empty} = \frac{K_{Cl}^2K_KK_{Na}k_f^{full}k_f^{empty}}{K_{Cl}^2K_KK_{Na}k_b^{full}}.$$

References

Arreola, J., Melvin, J.E., Begenisich, T., 1996. Activation of calcium-dependent chloride channels in rat parotid acinar cells. J. Gen. Physiol. 108, 35–47.

Atri, A., Amundson, J., Clapham, D., Sneyd, J., 1993. A single-pool model for intracellular calcium oscillations and waves in xenopus laevis oocyte. Biophys. J. 65, 1727–1739.

Benjamin, B.A., Johnson, E.A., 1997. A quantitative description of the Na-K-2Cl cotransporter and its conformity to experimental data. Am. J. Physiol. 273, F473–F482.

Berridge, M., 1995. Capacitative calcium entry. Biochem. J. 312, 1–11.

Berridge, M.J., Galione, A., 1988. Cytosolic calcium oscillators. FASEB J. 2, 3074–3082.

Bruce, J.I., Shuttleworth, T.J., Giovannucci, D.R., Yule, D.I., 2002. Phosphorylation of inositol 1,4,5-trisphoshate receptors in parotid acinar cells. A mechanism for the synergistic effects of cAMP on Ca^{2+} signaling. J. Biol. Chem. 277, 1340–1348.

Cook, D.I., Young, J.A., 1989a. Effect of K^+ channels in the apical plasma membrane on epithelial secretion based on secondary active Cl^- transport. J. Membrane Biol. 110, 139–146.

Cook, D.I., Young, J.A., 1989b. Fluid and electrolyte secretion by salivary glands. In: Forte, J. (Ed.), Handbook of Physiology, Section 6, vol. 3. Oxford University Press, Oxford, pp. 1–23.

Cooper, D.M., Mons, N., Karpen, J.W., 1995. Adenylyl cyclases and the interaction between calcium and cAMP signalling. Nature 374, 421–424.

De Young, G.W., Keizer, J., 1992. A single-pool inositol 1,2,5-trisphosphate-receptor-based model for agonist-stimulated oscillations in Ca^{2+} concentration. Proc. Natl Acad. Sci. USA 89, 9895–9899.

Domijan, M., Murray, R., Sneyd, J., 2006. Dynamical probing of the mechanisms underlying calcium oscillations. J. Nonlinear Sci. 16, 484–506.

Dupont, G., Goldbeter, A., 1993. One-pool model for Ca^{2+} oscillations involving Ca^{2+} and inositol 1,4,5-trisphosphate as co-agonists for Ca^{2+} release. Cell Calcium 14, 311–322.

Evans, R.L., Park, K., Turner, R.J., Watson, G.E., Nguyen, H.V., Dennett, M.R., Hand, A.R., Flagella, M., Shull, G.E., Melvin, J.E., 2000. Severe impairment of salivation in $Na^+/K^+/2Cl^-$-cotransporter (NKCC1)-deficient mice. J. Biol. Chem. 275, 26720–26726.

Foskett, J.K., 1990. $[Ca^{2+}]_i$ modulation of Cl^- content controls cell volume in single salivary acinar cells during fluid secretion. Am. J. Physiol. (Cell Physiol.) 259, C998–C1004.

Foskett, J.K., Melvin, J.E., 1989. Activation of salivary secretion: coupling of cell volume and $[Ca^{2+}]_i$ in single cells. Science 244, 1582–1585.

House, C.R., 1974. Water Transport in Cells and Tissues. E. Arnold, London.

Keizer, J., Levine, L., 1996. Ryanodine receptor adaption and Ca^{2+}-induced Ca^{2+} release-dependent Ca^{2+} oscillations. Biophys. J. 71, 3477–3487.

Lang, I., Walz, B., 2001. Dopamine-induced epithelial K^+ and Na^+ movements in the salivary ducts of *Periplaneta americana*. J. Insect Phys. 47, 465–474.

Läuger, P., Apell, H.J., 1986. A microscopic model for the current-voltage behaviour of the Na,K pump. Eur. Biophys. 13, 309–321.

Lytle, C., McManus, T., 1986. A minimal kinetic model of $Na + K + 2Cl$ cotransport with ordered binding and glide symmetry. J. Gen. Physiol. 88, 36a.

Ma, T., Song, Y., Gillespie, A.J.C., Epstein, C.J., Verkman, A.S., 1999. Defective secretion of saliva in transgenic mice lacking aquaporin-5 water channels. J. Biol. Chem. 274, 20071–20074.

Melvin, J.E., Yule, D., Shuttleworth, T., Begenisich, T., 2005. Regulation of fluid and electrolyte secretion in salivary gland acinar cells. Annu. Rev. Physiol. 67, 445–469.

Mignen, O., Thompson, J.L., Yule, D.I., Shuttleworth, T., 2005. Agonist activation of arachidonate-regulated Ca^{2+}-selective (ARC) channels in murine parotid and pancreatic acinar cells. J. Physiol. 564, 791–801.

Nauntofte, B., 1992. Regulation of electrolyte and fluid secretion in salivary acinar cells. Am. J. Physiol. 263, G823–G837.

Park, M.K., Lomax, R.B., Tepikin, A.V., Petersen, O.H., 2001. Local uncaging of caged Ca^{2+} reveals distribution of Ca^{2+}-activated Cl^- channels in pancreatic acinar cells. Proc. Natl Acad. Sci. USA 98, 10948–10953.

Politi, A., Gaspers, L.D., Thomas, A.P., Höfer, T., 2006. Models of IP_3 and Ca^{2+} oscillations: frequency encoding and identification of underlying feedbacks. Biophys. J. 90, 3120–3133.

Putney Jr., J.W., 1986. Identification of cellular activation mechanisms associated with salivary secretion. Annu. Rev. Physiol. 48, 75–88.

Raina, S., Preston, G.M., Guggino, W.B., Agre, P., 1995. Molecular cloning and characterization of an aquaporin cDNA from salivary, lacrimal, and respiratory tissues. J. Biol. Chem. 270, 1908–1912.

Romanenko, V., Nakamoto, T., Srivastava, A., Melvin, J.E., Begenisich, T., 2006. Molecular identification and physiological roles of parotid acinar cell Maxi-K channels. J. Biol. Chem. 281, 27964–27972.

Shuttleworth, T.J., Thompson, J.L., Mignen, O., 2004. ARC channels: a novel pathway for receptor-activated calcium entry. Physiology 19, 355–361.

Smith, N.P., Crampin, E.J., 2004. Development of models of active ion transport for whole-cell modelling: cardiac sodium-potassium pump as a case study. Prog. Biophys. Mol. Biol. 85, 387–405.

Sneyd, J., Dale, P.D., Duffy, A., 1998. Traveling waves in buffered systems: applications to calcium waves. SIAM J. Appl. Math. 58, 1178–1192.

Sneyd, J., Tsaneva-Atanasova, K., Bruce, J.I.E., Straub, S., Giovannucci, D., Yule, D.I., 2003. A model of calcium waves in pancreatic and parotid acinar cells. Biophys. J. 85, 1392–1405.

Sneyd, J., Tsaneva-Atanasova, K., Reznikov, V., Bai, Y., Sanderson, M.J., Yule, D.I., 2006. A method for determining the dependence of calcium oscillations on inositol trisphosphate oscillations. Proc. Natl Acad. Sci. 103, 1675–1680.

Takahata, T., Hayashi, M., Ishikawa, T., 2003. SK4/IK1-like channels mediate TEA-insensitive, Ca^{2+}-activated K^+ currents in bovine parotid acinar cells. Am. J. Physiol. Cell Physiol. 284, C127–C144.

Thaysen, J.H., Thorn, N.A., Schwartz, I.L., 1954. Excretion of sodium, potassium, chloride and carbon dioxide in human parotid saliva. Am. J. Physiol. 178, 155–159.

Thompson, J., Begenisich, T., 2006. Membrane-delimited inhibition of Maxi-K channel activity by the intermediate conductance Ca^{2+}-activated K channel. J. Gen. Physiol. 127, 159–169.

Tsien, R.W., Tsien, R.Y., 1990. Calcium channels, stores, and oscillations. Annu. Rev. Cell Biol. 6, 715–760.

Turner, R.J., Sugiya, H., 2002. Understanding salivary fluid and protein secretion. Oral Diseases 8, 3–11.

Turner, R.J., Paulais, M., Manganel, M., Lee, S.I., Moran, A., Melvin, J., 1993. Ion and water transport mechanisms in salivary glands. Crit. Rev. Oral Biol. Med. 4, 385–391.

Wagner, J., Keizer, J., 1994. Effects of rapid buffers on Ca^{2+} diffusion and Ca^{2+} oscillations. Biophys. J. 67, 447–456.

Wong, M.M.Y., Foskett, J.K., 1991. Oscillations of cytosolic sodium during calcium oscillations in exocrine acinar cells. Science 254, 1014–1016.